Journal of Physics D: Applied Physics

PAPER

Emergent properties in the natural composite $Ni_2MnSb_{0.5}Al_{0.5}$

To cite this article: Tamalika Samanta *et al* 2020 *J. Phys. D: Appl. Phys.* **53** 225302

IOP Publishing Journal of Physics D: Applied Physics
J. Phys. D: Appl. Phys. **53** (2020) 225302 (12pp) https://doi.org/10.1088/1361-6463/ab7c9f

Emergent properties in the natural composite $Ni_2MnSb_{0.5}Al_{0.5}$

Tamalika Samanta[1], D Salas[2], V Srihari[3], I Karaman[2] and P A Bhobe[1,4]

[1] Department of Metallurgy Engineering and Materials Science, Indian Institute of Technology Indore, Simrol, Indore 453 552, India
[2] Department of Materials Science and Engineering, Texas A & M University, College Station, TX, 77843, United States of America
[3] High Pressure and Synchrotron Radiation Physics Division, Bhabha Atomic Research Centre, 400 085 Mumbai, India
[4] Discipline of Physics, Indian Institute of Technology Indore, Simrol, Indore 453 552, India

E-mail: pbhobe@iiti.ac.in

Received 16 December 2019, revised 11 February 2020
Accepted for publication 4 March 2020
Published 31 March 2020

Abstract

We have investigated the structure, transport and magnetic properties of $Ni_2MnSb_{0.5}Al_{0.5}$ Heusler alloy. Structural analysis using x-ray diffraction and scanning electron microscopy has confirmed $Ni_2MnSb_{0.5}Al_{0.5}$ to be a *natural* composite of Ni_2MnSb and Ni_2MnAl phases, regardless of annealing conditions. This composite has a dendritic microstructure formed by the phase separation during solidification. The electronic phase separation was confirmed using x-ray near edge absorption spectroscopy, recorded at Mn and Ni K-edge and supported by *ab-initio* calculations of the same using multiple scattering theory. A thorough characterization of this novel composite form of $Ni_2MnSb_{0.5}Al_{0.5}$ Heusler alloy has been carried out by recording its magnetic and transport properties including electrical resistivity, thermal conductivity, and heat capacity. The composite micro-structure of this system plays a crucial role in drastically reducing its thermal conductivity value, while maintaining its metallic character. Unlike many oxide composites, the magnetic properties of the $Ni_2MnSb_{0.5}Al_{0.5}$ cannot be considered as the volume average of the characteristics of the two phases, rather it shows a long range ferromagnetic order with Curie temperature of 334 K and magnetic moment of 2.52 μ_B/f.u.

Keywords: x-ray diffraction, phase separation and segregation in solid solutions, XANES/EXAFS, electrical and thermal transport in crystalline materials

(Some figures may appear in colour only in the online journal)

1. Introduction

Nickel-manganese based Heusler alloys Ni-Mn-X, with X as a main group element, exhibit unique physical properties which originate from the interplay between structural and magnetic degrees of freedom [1]. Many of these alloys, either stoichiometric or off-stoichiometric, are known for exhibiting a variety of physical phenomena, like magnetic shape memory effect, magnetoelasticity, magnetic glass, strain glass, giant magnetoresistivity, and other multifunctional properties [2–7].

One such Ni–Mn based system is the stoichiometric Ni_2MnAl system, which displays superior mechanical properties and a stable structure down to the lowest temperatures. This system tends to stabilize into a dominant antiferromagnetic (AFM) B2 phase when quenched from a high temperature (~ 900 K). The ferromagnetic (FM) $L2_1$ phase in Ni_2MnAl starts to grow upon prolonged annealing [8]. It is difficult to produce a single $L2_1$ phase even after annealing at 653 K for more than 30 days as the diffusion kinetics are relatively slow in this compound as compared to the faster kinetics in other Ni_2MnX compounds such as Ni_2MnSb. This

latter compound readily stabilizes into an ordered $L2_1$ phase in which interaction is predominantly ferromagnetic (FM).

Tuning the Fermi level in the band structure by varying Ni-Mn-Sb alloy composition can enhance certain physical properties, such as Curie temperature and magnetic moment, leading to large magnetocaloric effect (MCE), and giant magnetoresistance (MR) [9, 10]. Having these facts in mind, we suggest that a quaternary Ni-Mn-Al-Sb alloy could hold the superior mechanical properties of Ni-Mn-Al alloys while stabilizing the $L2_1$ phase via Sb addition, leading to a predominant ferromagnetic behavior. Altogether, these properties may allow for new functional capabilities.

In this article, we have studied structure, resistivity, thermal conductivity and magnetic properties of a quaternary Heusler compound $Ni_2MnSb_{0.5}Al_{0.5}$. It has been observed that this alloy decomposes into two Heusler phases, Ni_2MnSb–enriched and Ni_2MnAl–enriched (below denoted as Sb–rich and Al–rich), after being synthesized by arc melting, turning into a natural composite. This phase-separation phenomenon is in thermal equilibrium, and does not simply produce chemical and electronic 'dirtiness/defects'. Rather it generates intricate interplay among charge/ spin/ lattice degrees of freedom leading to competing ground states with distinct electronic and magnetic properties. Besides, it has been shown that microstructural manipulation of several materials including many Heusler compounds, may notably change thermal transport properties often reducing their thermal conductivity, causing outstanding thermal properties [11, 12]. The stable, phase separated microstructure of $Ni_2MnSb_{0.5}Al_{0.5}$ indeed leads to a strong reduction of thermal conductivity compared to other quaternary Heuslers, owing to an enhanced scattering of phonons at the interfaces. These qualities make $Ni_2MnSb_{0.5}Al_{0.5}$ an ideal system to study the phase separation as a key to potential applications in practical engineering.

We have demonstrated that $Ni_2MnSb_{0.5}Al_{0.5}$ has a dendritic microstructure which was formed during the solidification process as a result of a phase separation into the two Heusler phases. The phase separation and its impact on the transport and magnetic properties of this composite alloy has been studied in detail. Though the alloy decomposes into two phases, it does not display any of the properties of the individual phases in magnetism, rather it shows a long range ferromagnetic order with Curie temperature of 334 K and magnetic moment of 2.52 μ_B/f.u., which also reflects in its electrical resistivity. Using x-ray near edge absorption spectroscopy (XANES) the electronic phase separation is studied. The composite microstructure of this system plays a crucial role in drastically reducing the thermal and electrical conductivity. Also, a significant phonon drag effect in the low temperature is seen. As a result an enhancement of thermal conductivity has been seen at low temperature.

2. Experimental details

Polycrystalline ingot with nominal $Ni_2MnSb_{0.5}Al_{0.5}$ at.% composition was prepared by arc-melting the stoichiometric ratio of elements ($\geq$99.99% purity) under argon gas atmosphere in a Tri-arc furnace with a water cooled copper crucible. The resulting alloy was subjected to the standard annealing treatment of heating for 48 hours at 800 °C, followed by quenching in ice-cold water. Selected samples, cut from the same ingot were subjected to different post-annealing heat treatments for investigating the effect of annealing temperature (400 to 1000 °C) and time (t = 1 to 24 hr) on the phase formation. Energy dispersive x-ray analysis (EDX) using SUPRA 55 Zeiss field emission scanning electron microscope was carried out to evaluate the composition at different spatial locations of the samples. The crystallographic structure was investigated by recording the x-ray diffraction (XRD) profile using the Cu K_α source and Bruker D8 Discover diffractometer. Synchrotron based powder XRD measurements at room temperature were also carried out on well ground powder samples at extreme conditions angle dispersive/energy dispersive x-ray diffraction (EC-AD/ED-XRD) beamline (BL-11) at Indus-2 synchrotron source, Raja Ramanna Centre for advanced Technology (RRCAT), Indore, India. These measurements were carried out in capillary mode and the capillary was rotated at 150 rpm to reduce the orientation effects. Desired wave length for AD-XRD diffraction experiments was selected using a Si(111) channel cut monochromator. The monochromatic beam was focused on to the sample with a Kirkpatrick-Baez mirror. Data was recorded using an image plate area detector. The sample to detector distance and the beam wavelength were calibrated using NIST standards LaB_6 and CeO_2.

The electrical resistivity and thermal transport and magnetization measurements were carried out using different attachments of a physical properties measurement system (PPMS) and a SQUID-based magnetometer, by Quantum Design Inc. The temperature was varied between 2 to 390 K and electrical resistivity was recorded in zero magnetic field and with 0.5 and 1 Tesla magnetic field. The magnetization as a function of field was measured at 5 K under sweep magnetic fields up to $\pm$8 T. Zero field cooled (ZFC) and field cooled (FCC) curves of magnetization were recorded in the range 5–600 K with an applied field of 100 and 500 Oe.

The x-ray absorption near edge spectra (XANES) experiments were carried out at the Mn and Ni K-edge at the applied x-ray absorption spectroscopy undulator beamline (P65) [13] of PETRA III, DESY, Hamburg, Germany. The experiments were performed in transmission mode and the incident and transmitted intensities were measured using gas-filled ionization chamber detectors. The experimentally obtained XANES are supported by *ab-initio* calculations of multiple scattering theory implemented by the FEFF9 code [14]. These calculations were performed adopting a cluster–size of 169 atoms and the Hedin-Lundqvist pseudopotential [15] to account for the exchange interactions. Self-consistent calculations were performed for a cluster radius of 7 Å.

3. Results and discussions

The B2-$L2_1$ degree of atomic order of the quaternary $Ni_2MnSb_{0.5}Al_{0.5}$ composition was analyzed using room

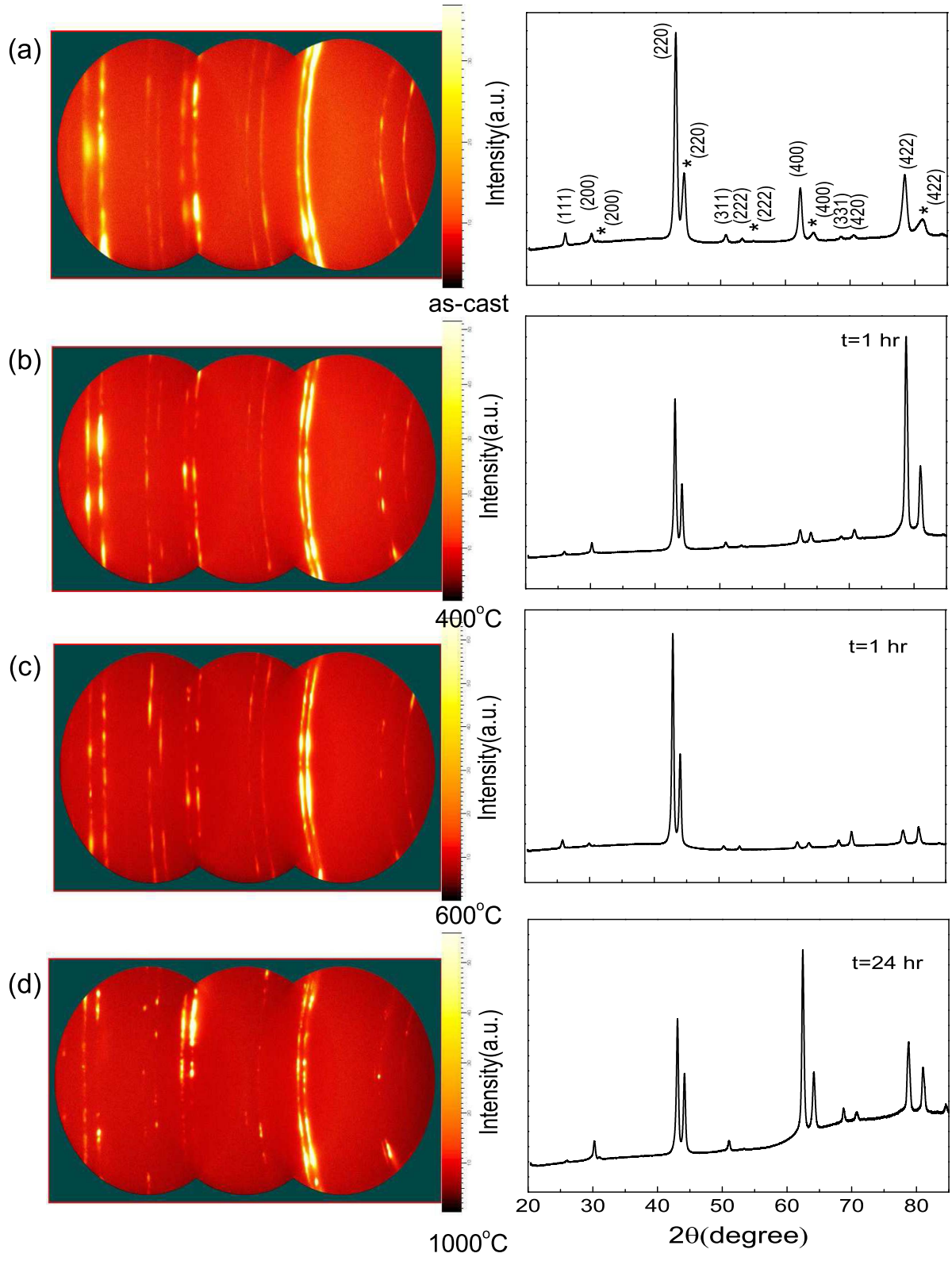

Figure 1. The room temperature powder XRD patterns of $Ni_2MnSb_{0.5}Al_{0.5}$ alloys in the (a) as-cast form and those subjected to different post annealing heat treatments of (b) 1 hr at 400 °C, (c) 1 hr at 600 °C and (d) 24 hr at 1000 °C (measured with CuK_α source). The two phases are identified as Ni_2MnSb-enriched phase (unmarked peaks) and the other is Ni_2MnAl-enriched phase (* marked peaks).

temperature powder x-ray diffraction (XRD) with Cu K-source. Figure 1 presents the diffraction patterns obtained for an as-cast (plain arc-melted) sample and those annealed with different thermal processing conditions: annealing at 800 °C for 48 hr then postannealing treatments performed at 400, 600 °C for 1 hr and 1000 °C for 24 hr. All diffraction patterns were satisfactorily fit to the sum of two cubic phases with different lattice parameters and state of order. Upon closer

inspection and analysis, the observed double peaks were traced back to two stable and separate phases, *viz*. Sb–rich Ni_2MnSb and Al–rich Ni_2MnAl, thus yielding a naturally formed composite material. As a consequence, order-independent peaks, like (220) peak around 44 °, appear as a doublet, while characteristic peaks of the ordered $L2_1$ phase, like (111) peak around 26°, may appear only for one of the cubic phases. For all four samples presented in figures 1(a)–(d), the ratio between the intensities of the two (220) peaks is similar. This fact indicates that annealing treatments did not have a significant impact on the volume fractions of the two phases, despite such treatments are expected to decrease internal stresses and anti-site disorder.

As observed from figure 1 it seems that any attempt to form a homogeneous composition of $Ni_2MnSb_{0.5}Al_{0.5}$ eventually results into a natural composite of Ni_2MnSb–enriched and Ni_2MnAl–enriched alloys, regardless of annealing temperature and time. Furthermore, changing the atomic ratio of Sb to Al from 50:50 to any other value is expected to decrease the stability of the solid solution in favor to the ternary compounds. Consequently, all further characterization reported here has been carried out on the 50:50 composition, annealed at 800 °C for 48 hr before quenching in ice water (without any postannealing treatments).

The phase separation was corroborated using scanning electron microscope (SEM). Figure 2 shows a FE-SEM micrograph for the $Ni_2MnSb_{0.5}Al_{0.5}$ system. The material presented a clear dendritic microstructure. The dendritic structures are formed through constitutional supercooling during alloy solidification. Factors such as degrees of supercooling, a liquidus temperature gradient typically resulting from a composition gradient, velocity of the solid -liquid interface vastly affect the dendritic formation [16]. Dendritic growths are also known to increase the ductility of a system [17]. In the case of $Ni_2MnSb_{0.5}Al_{0.5}$, the phase separation into full Heusler cubic Ni_2MnAl and Ni_2MnSb takes place during the arc-melting process itself, as confirmed from its XRD plots. The annealing process allows the two phases to relax any strain in the crystal structure while in liquidus phase, whereas, a slight difference in the solidification temperature of the two phases leads to the growth of the dendritic structures.

From EDX measurements the average compositions of the dark dendrites (low Z contrast) was found to be Al rich $Ni_{2.04}Mn_{0.93}Al_{0.97}Sb_{0.06}$, whereas bright matrix (high Z contrast) composition was Sb rich $Ni_{1.98}Mn_{1.02}Sb_{0.89}Al_{0.11}$. These phases are quite homogeneous (measurements presented a standard deviation of 3%) and are close to the ternary Heusler Ni_2MnAl and Ni_2MnSb compositions. The dendritic morphology in figure 2 suggests that, during the solidification process, first Ni_2MnAl nucleated out of the liquid phase, precipitating most of the aluminium, and then Ni_2MnSb solidified forming the matrix. This morphology may thus be taken as a hint to phase separation by nucleation and growth in contrast to a spinodal decomposition [12].

In order to identify the exact crystallographic details of the two phases, room temperature x-ray diffraction using high intensity synchrotron radiation ($\lambda = 0.62\,869$ Å) was performed on a powdered sample (annealed at 800 °C for 48 hr before quenching in ice water). Such a diffraction profile is presented in figure 3(a), and contrasted against the calculated patterns of the ternary Ni_2MnAl and Ni_2MnSb phases. Each reflection observed in the experimental pattern could be mapped to the individual simulated pattern of Ni_2MnSb and Ni_2MnAl phases. The (111) superlattice reflection is clearly absent for the Ni_2MnAl phase, whereas both, (111) and (200) reflections are present for Ni_2MnSb phase. The absence of the (111) superlattice reflection is a signature of B2 type site-disorder in the Al–rich phase. The quantitative analysis carried out using the Rietveld refinement method and implemented through the FULLPROF [18] suite confirms the symmetry in the crystal structure, as presented in figure 3(b). The unit cell parameters are found to be 5.961 7(1) Å for the Sb–rich phase and 5.821 3(2) Å for the Al–rich phase. The magnified view of *220* peak of the system in inset of figure 3(b) presents the clear splitting caused by the phase separation into two Heusler compositions with different lattice constants. Rietveld analysis estimates the volume fraction of the Sb rich and Al rich phase to be 65% and 35% respectively. However, this quantitative phase fractions could be misleading as the fitted model gets quite complicated with further incorporation of $L2_1$+B2 state of Ni_2MnAl. Another technique such as neutron diffraction can be helpful here.

Understanding of other physical properties of the natural composite of $Ni_2MnSb_{0.5}Al_{0.5}$ becomes pertinent as it encompasses a possibility of emergent phenomena resulting from its nature as a composite. We begin with the inspection of the magnetic properties investigated through dc magnetization (M) measurements, and carried out as a function of temperature and applied magnetic field. From figure 4(a) it is seen that the M(T) curve of $Ni_2MnSb_{0.5}Al_{0.5}$ composite is a single continuous or second order transition from paramagnetic to a magnetically ordered state. Interestingly, a $T_C \sim 334$ K is obtained from the ZFC curve, while a shift to ~ 332 K is observed for the FCC curve, as conveyed from the *dM(T)/dT* plot displayed in the inset of figure 4(a). Furthermore, below T_C, the FCC curve appears to be temperature-independent, as would be expected from a ferromagnetic material. By contrast, the ZFC curve seems to have a gradually rising slope in the direction of increasing temperature. A clear bifurcation in the ZFC and FCC curve exists over the entire low temperature range, and extends much beyond T_C (up to ~ 350 K). Application of a slightly higher magnetic field of 500 Oe (see figure 4(b)) does not seem to affect this ZFC/FCC hysteresis, but the sharpness of the transition gives way to a smooth rounded downturn, once again mimicking a situation typical of a ferro/ferri–magnetic material.

Altogether, these observations in the M(T) behavior are indicative of a mixed FM/AFM interactions that seem to originate from the two underlying structural phases. Consequently, the question that arises is, whether the two structural phases in the composite $Ni_2MnSb_{0.5}Al_{0.5}$ interact magnetically or is it just the combined behavior of the two separate magnetic phases? To answer this, we refer back to the magnetic heterogeneity of the two constituent phases. As per the reports present in literature, Ni_2MnSb is a

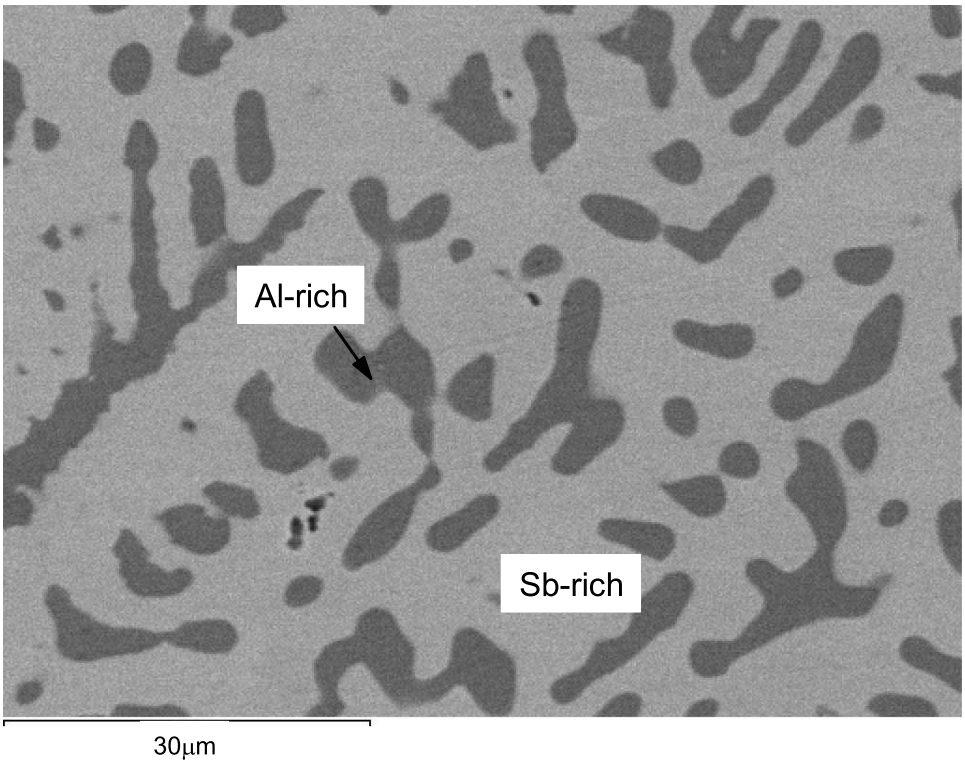

Figure 2. FE-SEM image of $Ni_2MnSb_{0.5}Al_{0.5}$ composite (annealed at 800 °C for 48 hr) taken from a polished surface.

ferromagnet [19, 20] with Curie temperature (T_C) of ~ 380 K and a saturation magnetization value of ~ 3.9 μ_B/f.u. On the other hand, the *B2* phase of Ni_2MnAl displays a Néel temperature of 313 K and fails to saturate even after application of sufficiently high magnetic field [8, 21]. Also, it is pertinent to mention that the least stable $L2_1$ phase of Ni_2MnAl orders ferromagnetically at T_C ~ 375 K [8]. As stated earlier from the XRD results of the composite, the Al–rich phase comprises of a dominating *B2* phase and hence would contribute antiferromagnetic (AFM) order. Evidently, the T_C for composite system does not match with the ordering temperatures seen in either of the individual Heusler phases, which is an uncommon result for a composite. For example, in case of the Heusler composites $Co_2Mn_{1-x}Ti_xSn$ ($0 \leq x \leq 1$), the Mn–rich phase and Ti–rich phase show two magnetic phase transitions which can be correlated with the different Curie temperatures of the phases [12].

A Curie–Weiss (CW) fit to M(T) in the high temperature region (500 - 600 K) presented in figure 4(c), yields a Curie–Weiss temperature θ_{CW} ~ 380±4 K. A difference of about 45 K between the T_C and θ_{CW} suggests that magnetic correlations start to build up much before its ordering temperature. Furthermore, the paramagnetic moment extracted from Curie–Weiss fit is about 1.16±0.01 μ_B/f.u., while the saturation magnetization of 2.52 μ_B/f.u. is obtained from the isothermal magnetization, M(H), recorded at 5 K (see figure 4(d)). In addition, the M(H) curve rises rapidly at low fields until 0.3 T, but instead of readily attaining a saturation value thereafter, the M(H) curve shows a very slow and steady increase from 0.3 to 8 T. The coexistence of AFM phase is the essential source for this non–saturation, while the overall M(H) hysteresis depicts a soft ferromagnetic-like behavior.

Neither the T_C nor the saturation magnetization (and paramagnetic moment) values match with that of the individual Heusler phases of the composite. The overall results suggest that the Al-rich and Sb-rich phases are not magnetically independent, but their mutual magnetic interaction configures the magnetic behavior of the composite. When viewed from the high temperature side, the magnetic interactions in both the phases of the composite start at ~ θ_{CW}, and intensify as the system temperature is lowered. However, the opposing magnetic interactions in the two phases has a considerable effect on the pinning of the spin configurations. The up-spins of the AFM Al–rich phase pins with the up-spins of Sb–rich phase, thus hindering the establishment of long range order in either of the phases. As the temperature is lowered, the pinning interactions intensifies and so does the local magnetic interactions within the grains of individual phases. As a result of this magnetic interaction between the two crystallographic phases a new ordering temperature (T_C) is obtained for the composite. The magnetic behavior of the individual phases is masked by such an interaction and the structural composite behaves as a single magnetic entity.

Next, the four-probe electrical resistivity was measured in the temperature range from 2 K to 390 K, thus spanning the magnetic ordering temperature of the composite. Figure 5 shows the data obtained in the heating and cooling cycles and reveals a metallic behavior ($\frac{d\rho}{dt} > 0$) in the entire temperature range. There is no hysteresis in the resistivity data between heating and cooling ramps. Notably, a pronounced change

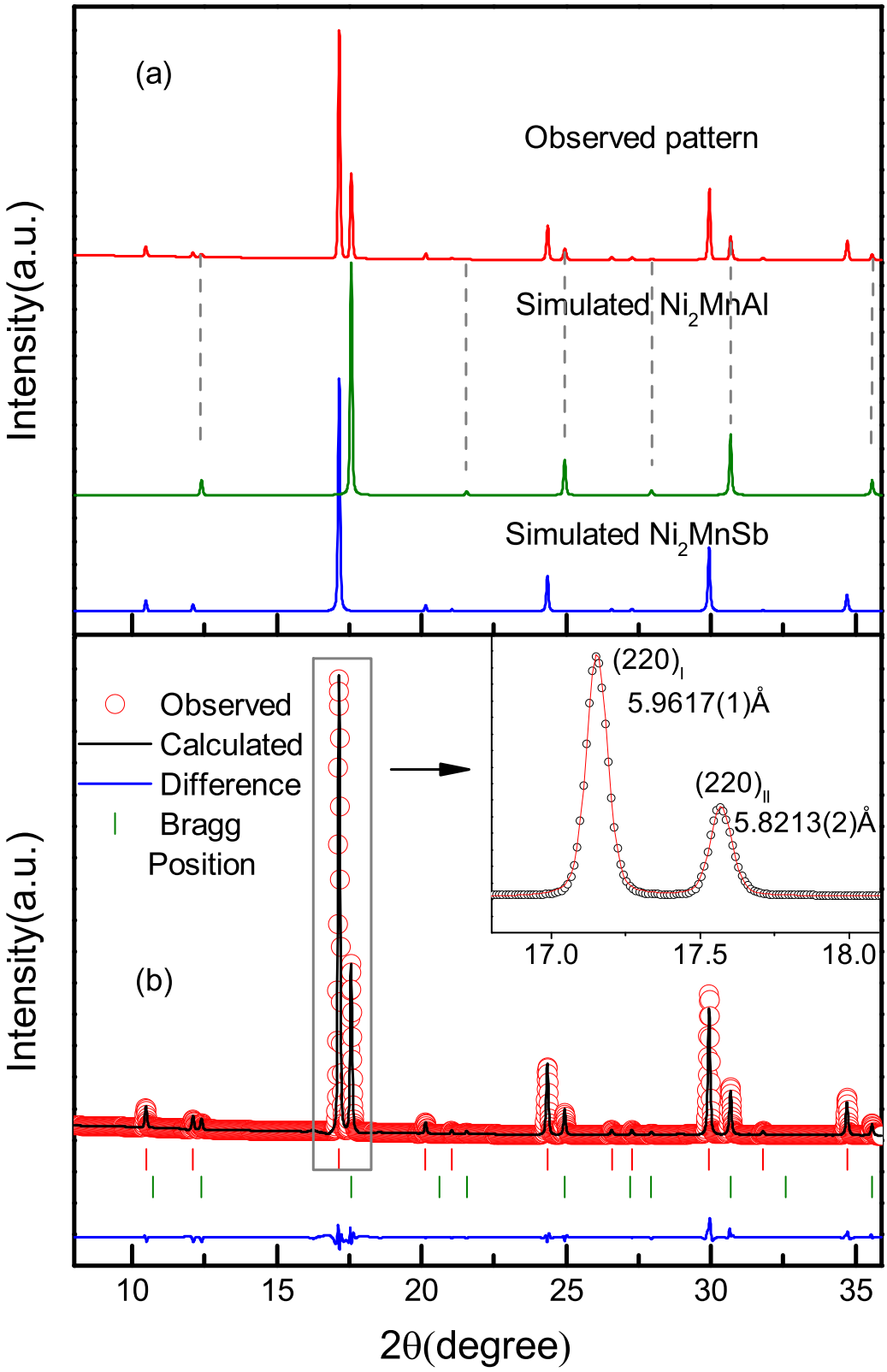

Figure 3. (a) The simulated patterns of Ni_2MnSb-enriched and Ni_2MnAl-enriched phases compared with the experimental XRD pattern measured at synchrotron source with $\lambda = 0.62\,869$ Å. (b) The Rietveld refinement of the powder XRD pattern of $Ni_2MnSb_{0.5}Al_{0.5}$. Inset shows the 220 peak of the two phases with different lattice constants.

in the temperature dependence of the slope of resistivity is observed in the region of the Curie temperature. Following, the material's electrical resistivity was recorded during thermal cycles under a constant applied magnetic field of 0.5 and 1 T. The variation of ρ(T) was mostly magnetic field independent. However, a small but systematic resistivity reduction with

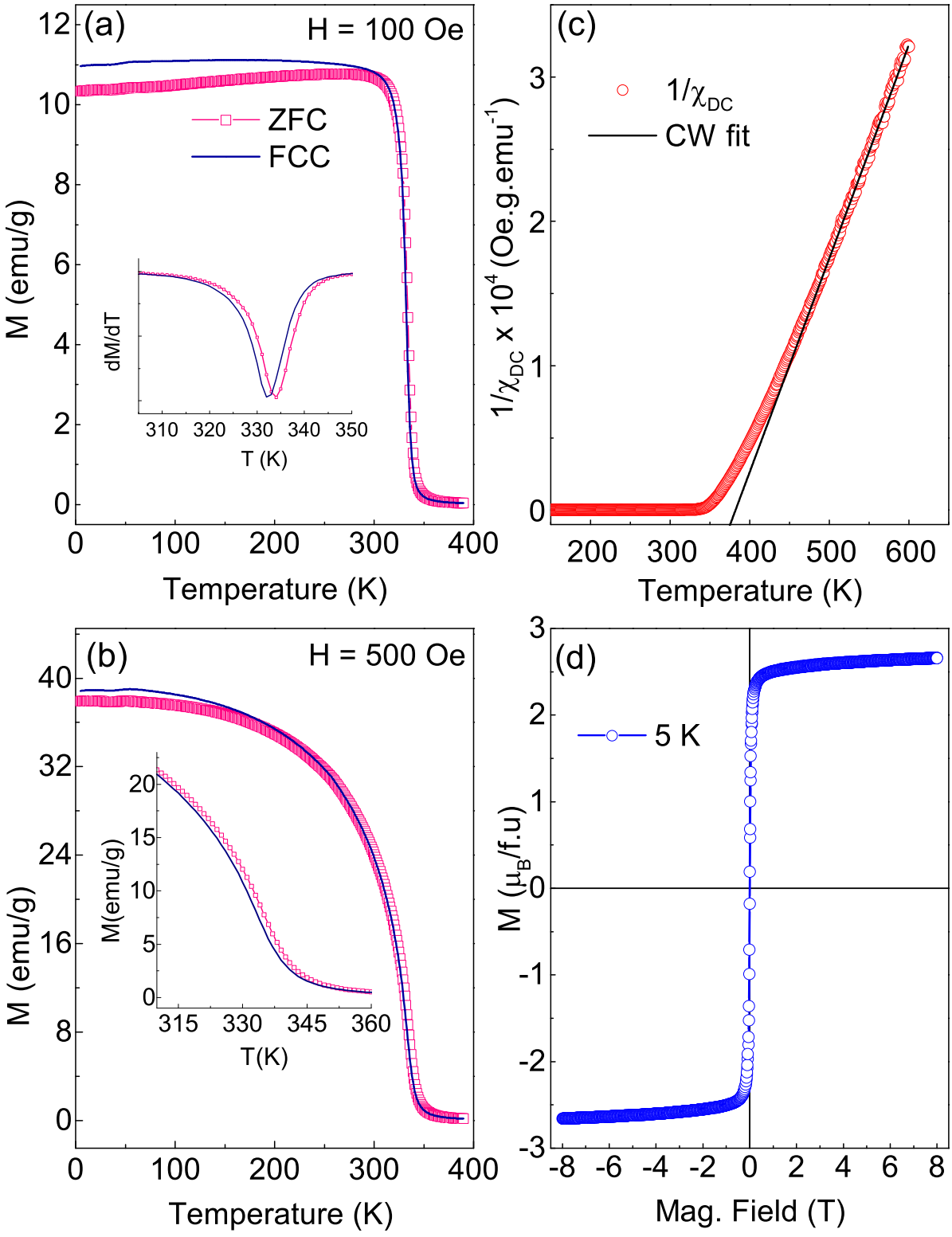

Figure 4. Temperature dependent magnetization of $Ni_2MnSb_{0.5}Al_{0.5}$, measured in the zero field cooled warming (ZFC) and field cooled cooling (FCC) protocols, under an applied magnetic field of (a) 100 Oe (top panel) and (b) 500 Oe (bottom panel). T_C was determined from the temperature derivative of M(T), as shown in the inset of (a). The inset in (b) shows the ZFC/FCC bifurcation under 500 Oe field at high temperatures. (c) The inverse susceptibility, extracted from $M(T)$ *vs.* T, measured with a field of 500 Oe and upto 600 K, fitted with the Curie–Weiss (CW) law (black line). (d) Field dependence of magnetization recorded at 5 K.

magnetic field was observed in the vicinity of the Curie temperature, as can be seen in the inset of figure 5. The systematic decrease of resistivity with increasing magnetic field indicates that the ferromagnetic pinning between the FM and AFM grains within the material is reinforced, and scattering of charge carriers decreases.

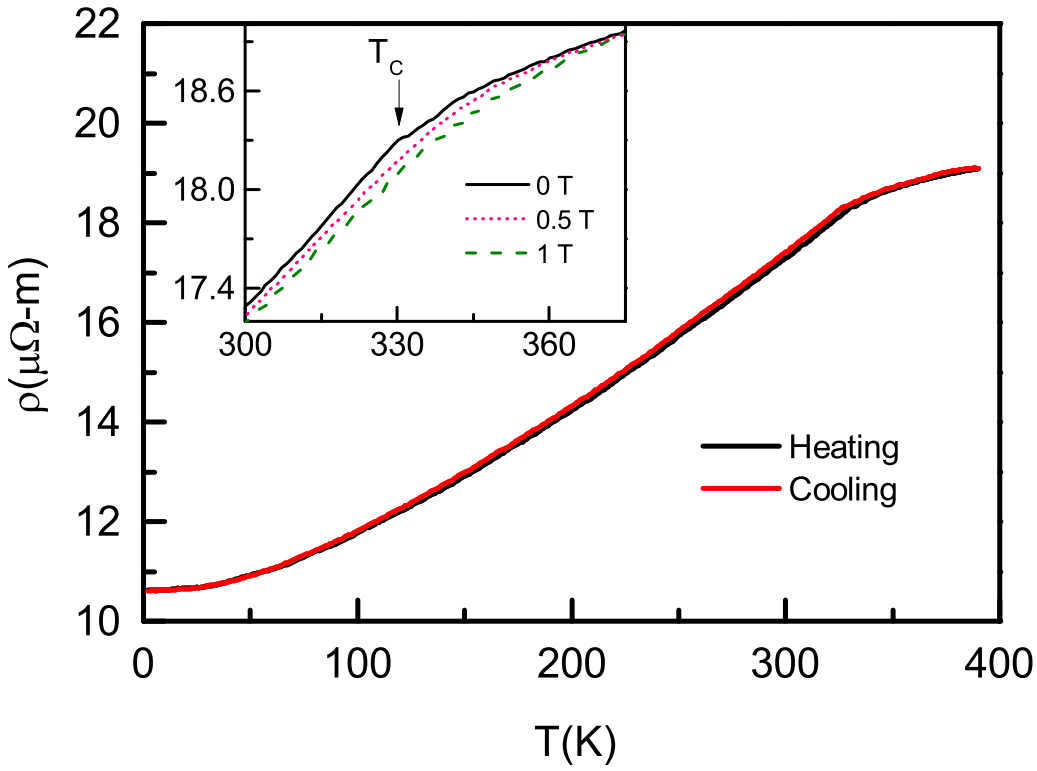

Figure 5. Electrical resistivity of $Ni_2MnSb_{0.5}Al_{0.5}$ in zero field during heating and cooling cycles. Inset: resistivity data in applied magnetic field of 0 T, 0.5 T and 1 T in the vicinity of T_C.

The absolute magnitude of resistivity, though, is found to be quite high compared to typical metals [22] with residual resistivity at 2 K ~ 10.6 $\mu\Omega$-m. This result is expected due to the static factors like local lattice strains formed in the phase boundaries and heterogeneous electronic band structure. XANES is a simple and sensitive probe of the local unoccupied density of states (DOS). This technique can provide intricate information related to the modification of DOS of the selected absorbing atomic species. Since the most prominent contribution to the DOS at the Fermi level of Heuslers comes from its 3*d* bands, Mn and Ni K-edge spectra of $Ni_2MnSb_{0.5}Al_{0.5}$ composite were recorded, as shown in figure 6. These spectra were contrasted with the theoretical XANES spectra of Ni_2MnSb and Ni_2MnAl compounds, which were calculated using the *ab-initio* FEFF9 code [14]. The main features are denoted as *A*, *B*, *C* for Ni edge and *D*, *E*, *F* for Mn edge spectra. As can be seen in figure 6, a feature by feature mapping of the two individual phases of Ni_2MnSb and Ni_2MnAl is seen with the experimental spectra. This fact points towards the presence of the individual band structures or in other words, the separate electronic phases in the composite.

In order to evaluate the potential applications of the present phase separated material, thermal conductivity, κ_T, of the composite was measured as a function of temperature during heating and it is shown in figure 7. Thermal conductivity was observed to be significantly small. Generally in intermetallics the value of κ_T remains within 5 ~ 6 W/K-m at room temperature, though in systems with phase separated microstructure, this value tends to decrease to 2-3 W/K-m [12]. However, we obtained a value below 1.6 W/K-m at 273 K for the current composite. Such enormous reduction in κ_T by more than 50% can be understood by a distinct influence of the phase boundaries. The boundary scattering of low-frequency phonons, which are responsible for transporting heat in a solid solution occurs at the interfaces between Sb-rich and Al-rich phases. It is expected that both grain and phase boundaries present lower atomic order and atomic density, which should strongly increase the materials thermal resistance in the entire temperature range [23]. Therefore, the observed low thermal conductivity could be associated with a high planar defect density in this system.

To study the impact of the phase separation on the thermal properties in more detail, κ_l, which is the lattice contribution to thermal conductivity, needs to be separated from the electronic contribution, κ_e. According to Wiedemann-Franz law, the electronic thermal conductivity can be expressed as $\kappa_e = \sigma LT$, being σ the electrical conductivity, L the Lorenz number (2.44×10^{-8} W Ω K^{-2}), and T the temperature. Subsequently, the lattice thermal conductivity has been calculated by subtracting the electronic contribution from the total thermal conductivity. Both contributions are displayed in figure 7. A comparison of κ_l with κ_T at 280 K indicates that the lattice contribution to thermal conductivity is the most dominant among the contributions ($\kappa_l/\kappa_T \sim 74\%$). The electronic conductivity increases monotonically with temperature, giving a gradual increment in the total conductivity at high temperatures. The lattice thermal conductivity can be defined by $\kappa_l = c_v vl$ [24], where c_v is the phonon specific heat, v represents the phonon drift velocity, and l is the mean free path. The phonon drift velocity and mean free path are expected to be

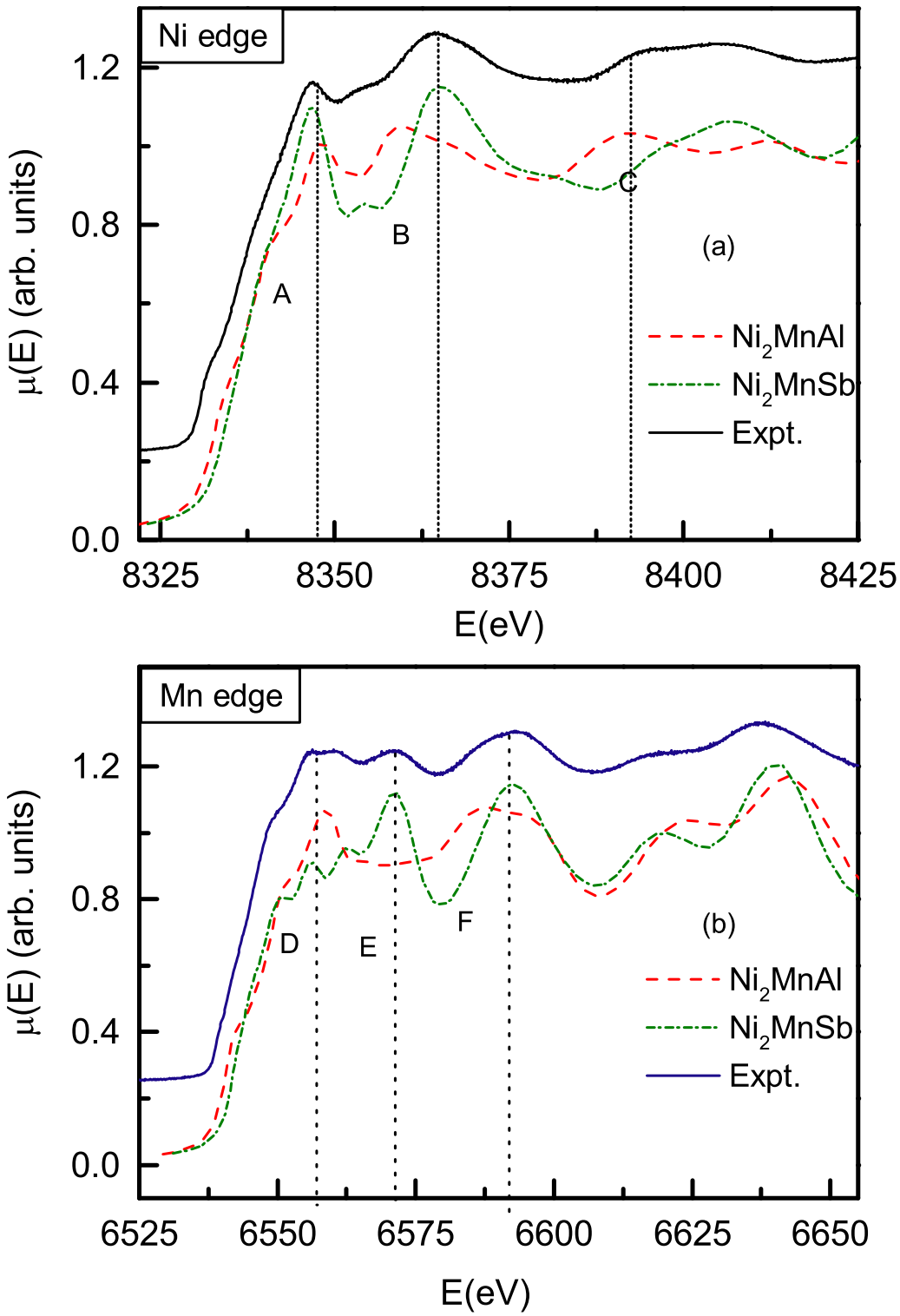

Figure 6. Theoretical XANES spectra for Ni_2MnSb and Ni_2MnAl in comparison with the experimental XANES spectra of $Ni_2MnSb_{0.5}Al_{0.5}$ alloy at (a) Ni edge and at (b) Mn edge.

greatly influenced by the microstructure of this system, in turn affecting the lattice thermal conductivity. Moreover, for a system which displays a metallic electrical resistivity, ideally the free electrons, interacting with the lattice waves, should limit the phonon mean free path, making the contributions of κ_e stronger than κ_l. This is not the scenario in the present case. It is clear that the phase separation plays the key role in exhibiting a higher resistivity and in turn a lower electronic contribution to the thermal conductivity. For an application of such phase separation in thermoelectric materials, the ratio of κ_e to κ_l needs to be adjusted and proposed to be 0.5 for an optimization of the thermoelectric figure of merit [25].

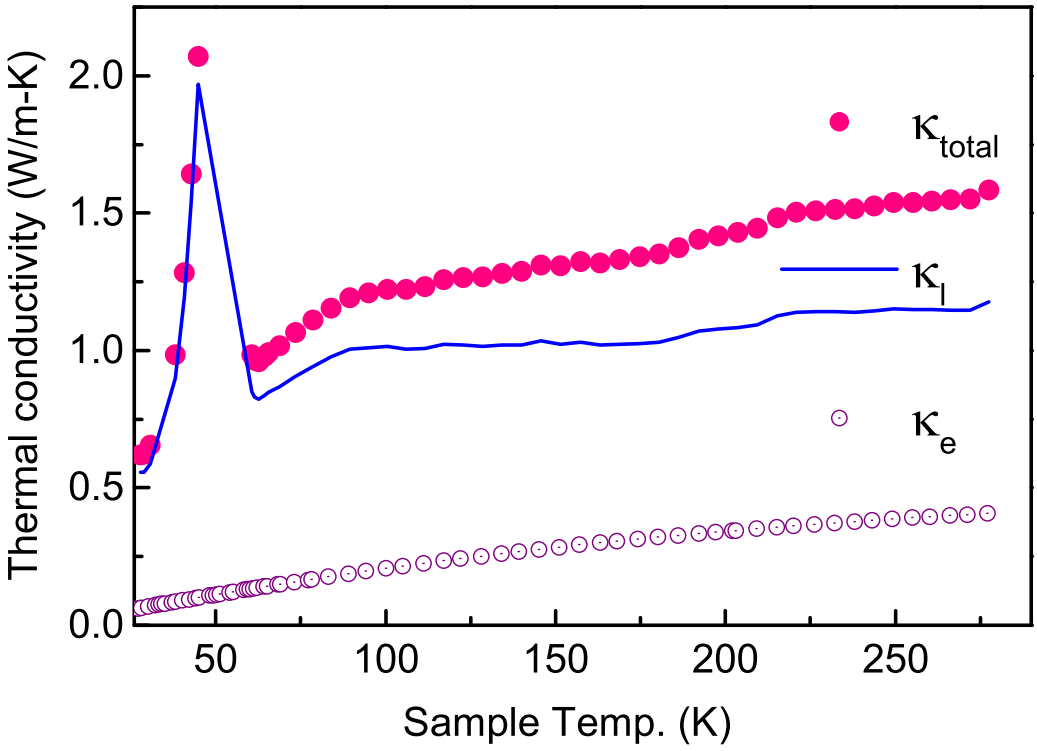

Figure 7. Total thermal condutivity, κ_T, Lattice thermal conductivity, κ_l and electrical thermal conductivity κ_e of $Ni_2MnSb_{0.5}Al_{0.5}$.

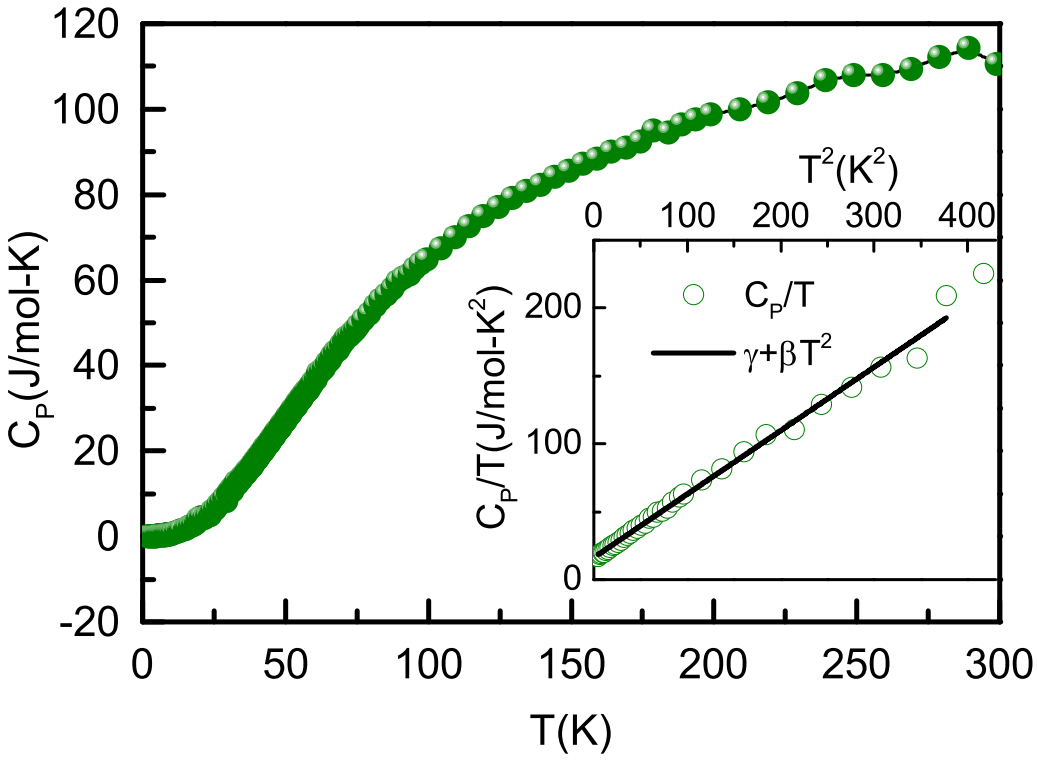

Figure 8. (a) Specific heat capacity, C_P variation with temperature in the range 2–300 K of $Ni_2MnSb_{0.5}Al_{0.5}$ alloy. Inset: C_P/T *vs.* T^2 plot and the Debye-Weller fit to the low temperature data in the range 2–20 K.

In figure 7, κ_T presents a spike-like feature near 45 K. To elucidate the origin of this feature, we proceed to explore the likelihood of a phase transition occurring at low-temperatures by recording the temperature dependence of the heat capacity ($C_P(T)$) of the composite. Since the specific heat of the alloy should be sensitive to processes involving entropy change, the

existence of any kind of transition in the composite system could be unambiguously detected. Figure 8 depicts the $C_P(T)$ *versus* temperature (T) plot. The heat capacity does not show any jumps or kinks over the entire temperature range ruling out the possibility of any phase transition. At low temperature, $C_P(T)$ can be described by the typical behavior of Debye—T^3 law, where $C_P(T) = \gamma T + \beta T^3$. Here γ and β are the coefficients of electronic and lattice specific heat, respectively. The Debye temperature, θ_D, calculated from β is found to be ~255 K. The value of γ is 16.2 mJ/mol-K^2. The fitting in the temperature range 2–20 K is shown in the inset of figure 8.

Having excluded the possibility of any structural phase transition occurring at 45 K, the non–monotonic behavior of $\kappa_T(T)$ can be analyzed in terms of a positive phonon drag effect, wherein a preferential scattering of the charge carriers takes place in the direction channelized by the phonons streaming from hot to cold end in thermal conduction. It is mostly evidenced at low temperatures where the phonon mean free path becomes longer. Such behavior is known to affect meaningfully the thermopower of different materials, including single crystals of Ge [26], Si [27], and $CrSb_2$ [28], nanocomposites of $FeSb_2$ [29]. In a rough approximation, $T_p \approx \theta_D/5$, where T_p is the temperature where phonon drag occurs and θ_D is the Debye temperature. For this system T_p occurred at 45 K and Debye temperature was found to be 255 K, which supports the scaling between T_p and θ_D.

Keeping in view the interesting electrical resistivity and thermal conductivity results, several attempts were made to measure the thermopower of the composite system. Each time, the absolute value of the Seebeck coefficient was found to be small ($|S| < 2\mu$V/K) and consistently fluctuating around zero. The scattering of charge carriers at grain boundaries of the two structural phases could give rise to such values of S, it is equally possible that opposing contributions coming from the Sb–rich and Al–rich phases could cancel the resultant S. As there are no previous reports of thermopower measurements on individual Ni_2MnSb and Ni_2MnAl systems, it is difficult to comment further. In future, it would be interesting to investigate the behavior of S in individual phases and its contribution to the composite $Ni_2MnSb_{0.5}Al_{0.5}$ system.

4. Conclusions

To summarize, in this paper we have studied a Heusler composite $Ni_2MnSb_{0.5}Al_{0.5}$ through structural, magnetic, electrical, and thermoelectrical properties. This material decomposes into two Heusler–like phases Ni_2MnSb and Ni_2MnAl, as confirmed by high resolution x-ray measurements and EDX compositional analysis. This phase separation leads to a distinct dendritic microstructure as detected from FESEM. The electronic phase separation has also been proved experimentally by x-ray absorption near edge studies. DC magnetization studies on the compound reveal a magnetic behavior where the individual phases seem to interact magnetically resulting a single continuous magnetic transition from paramagnetic to a magnetically ordered state. The electrical resistivity reflects a metallic nature with high residual resistivity due to the heterogeneous phase. Also, the thermal conductivity have been analyzed qualitatively and found to have several indicators of the presence of substantial electron–phonon interaction at low temperature. Further, phonon scattering processes at phase boundaries lead to a pronounced reduction in the lattice thermal conductivity compared to a single-phase system.

Acknowledgment

We are grateful to Professor A K Nigam, TIFR, Mumbai for extending measurement facilities to us, and Mr D Buddhikot, TIFR for his help in measurements. Parts of this research were carried out at the light source PETRA III at DESY, a member of the Helmholtz Association (HGF) and we thank Edmund Welter for assistance in using the photon beamline P65. We acknowledge financial support provided by the Department of Science and Technology (Government of India, India@DESY collaboration). This work is partially supported by Science and Engineering Research Board (SERB), India through Grant No: EMR/2017/001425. P A B thanks Department of Science and Technology (DST), Government of India and Indo-US Science and Technology Forum (IUSSTF) for Women in STEMM Overseas Fellowship Programme 2018. D S and I K acknowledge the support from National Science Foundation (NSF), Division of Materials Research, Metals and Metallic Nanostructures Program, under the Grant No. DMR-1905325.

ORCID iDs

Tamalika Samanta https://orcid.org/0000-0002-1202-8348
P A Bhobe https://orcid.org/0000-0002-6267-0005

References

[1] Acet M, Nosa L M and Planes A 2011 Magnetic-field-induced effects in martensitic Heusler-based magnetic shape memory alloys *Handbook of Magnetic Materials* (New York: Elsevier) vol 19 ch 4
[2] Krenke T, Acet M, Wassermann E F, Moya X, Manosa L and Planes A 2006 *Phys. Rev.* B **73** 174413
[3] Krenke T, Çak ir A, Scheibel F, Acet M and Farle M 2016 *J. Appl. Phys.* **120** 243904
[4] Bhobe P A, Monteiro J H, Cascalheira J C, Mendiratta S K, Priolkar K R and Sarode P R 2006 *J. Phys. Condens. Matter* **18** 10843
[5] Monroe J, Karaman I, Basaran B, Ito W, Umetsu R, Kainuma R, Koyama K and Chumlyakov Y 2012 *Acta Mater.* **60** 6883–6891
[6] Monroe J, Raymond J, Xu X, Nagasako M, Kainuma R, Chumlyakov Y, Arroyave R and Karaman I 2015 *Acta Mater.* **101** 107–115
[7] Stonaha P J *et al* 2018 *Phys. Rev. Lett.* **120** 245701
[8] Acet M, Duman E, Wassermann E F, Maosa L and Planes A 2002 *J. Appl. Phys.* **92** 3867–3871
[9] Khan M, Dubenko I, Stadler S and Ali N 2008 *J. Phys. Condens. Matter* **20** 235204
[10] Khan M *et al* 2013 *Appl. Phys. Lett.* **102** 112402
[11] Sakurada S and Shutoh N 2005 *Appl. Phys. Lett* **86** 082105

[12] Graf T, Barth J, Blum C G F, Balke B, Felser C, Klaer P and Elmers H J 2010 *Phys. Rev.* B **82** 104420
[13] Welter E, Chernikov R, Herrmann M and Nemausat R 2019 *Conf. Proc.* **2054** 040002
[14] Rehr J J, Kas J J, Vila F D, Prange M P and Jorissen K 2010 *Phys. Chem. Chem. Phys.* **12** 5503–13
[15] Hedin L and Lundqvist B I 1971 *J. Phys. C: Solid State Phys.* **4** 2064–83
[16] Porter D A, Easterling K E and Sherif M Y 2009 *Phase Transformations in Metals and Alloys* (Boca Raton, FL: CRC Press)
[17] He G, Eckert J, Loser W and Schultz L 2003 *Nat. Mat.* **2** 33
[18] Rodrguez-Carvajal J 1993 *Physica* B **192** 55–69
[19] Khan M, Dubenko I, Stadler S and Ali N 2008 *J. Phys. Condens. Matter* **20** 235204
[20] Szytua A, Koodziejczyk A, Rzany H, Todorovi J and Wanic A 1972 *Phys. Status Solidi* a **11** 57–65
[21] Galanakis I and Şaşioglu E 2011 *Appl. Phys. Lett.* **98** 102514
[22] Giancoli D C 1995 *Physics* 4th edn (Englewood Cliffs, NJ: Prentice Hall)
[23] Klemens P G 1994 *Int. J. Thermophys.* **15** 1345
[24] Bodzenta J 1999 *Chaos Solitons Fractals* **10** 2087–98
[25] Bhandari M C 1995 *CRC Handbook of Thermoelectrics* (Boca Raton: CRC Press)
[26] Geballe T H and Hull G W 1954 *Phys. Rev.* **94** 1134–1140
[27] Geballe T H and Hull G W1955 *Phys. Rev.* **98** 940–7
[28] Sales B C, May A F, McGuire M A, Stone M B, Singh D J and Mandrus D 2012 *Phys. Rev.* B **86** 235136
[29] Pokharel M, Zhao H, Lukas K, Ren Z, Opeil C and Mihaila B 2013 *MRS Commun.* **3** 31–6